JME

Journal of Mining & Environment,
Vol.9, No.1, 2018, 169-182.
DOI: 10.22044/jme.2017.5950.1408

Long-term stability analysis of goaf area in longwall mining using minimum potential energy theory

M. Rezaei

Department of Mining Engineering, Faculty of Engineering, University of Kurdistan, Sanandaj, Iran

Received 29 June 2017; received in revised form 14 August 2017; accepted 19 August 2017
Corresponding author: m.rezaei@uok.ac.ir (M. Rezaei).

Abstract
Estimation of the height of caved and fractured zones above a longwall panel along with the stability conditions of the goaf area are very crucial to determine the abutment stresses, ground subsidence, and face support as well as designing the surrounding gates and intervening pillars. In this work, the height of caving-fracturing zone above the mined panel is considered as the height of destressed zone (HDZ). The long-term estimation of this height plays a key role in the accurate determination of maximum ground surface subsidence and the amount of transferred loads towards the neighbouring solid sections. This paper presents a new stability analysis model of caved material system in the goaf area. For this aim, a theoretical energy-based model of HDZ determination in long-term condition is developed. Then the stability condition of the caved material system is investigated using the principle of minimum potential energy. On the basis of the actual data gathered from the literature, the unstable time period of the caved material system is also calculated. Moreover, the effects of time- and temperature-related parameters and constant coefficients as well as their inherent relations with HDZ are evaluated. Furthermore, sensitivity analysis shows that the two temperature-related constants material constant and time are the most effective variables in HDZ, and the slope of material hardening is the least effective one. The estimated HDZ and the stability time of the caved materials can be successfully applied to determine the induced stress and the maximum surface subsidence, respectively, due to longwall mining.

Keywords: *Longwall Mining, Height of Destressed Zone, Caved Material System, Minimum Potential Energy, Stability Time.*

1. Introduction

Longwall mining method is one of the most popular and productive underground methods used in the mining industry. This method is suitable for extraction of the relatively thick, sub-horizontal, and uniform coal (rock) seams. The main objective of this method application is high productivity along with providing the acceptable safety conditions. However, the mining efficiency exclusively depends upon the stability of the stopes, gates, surrounding access tunnels, and pillars. The stability of these structures is also related to both the roof cave-in performance and the interaction of the caved materials with the roof rock strata. Subsequent to the seam extraction and advancing the hydraulic jacks, the immediate roof in the mined area collapses and caves at the rear of the working face. The downward movement of the roof rock strata then gradually extends upwards and will cause the disturbed roof strata to become destressed. Thus the overburden pressure above the destressed zone will be redistributed in the rock mass surrounding the longwall panels and directed to the front and rib-side abutments [1-7].

Generally, there are several research approaches to study the progressive fracturing and caving of the panel roof rock strata including in-situ measurement as well as physical, empirical, numerical, and analytical modeling. Despite being worthy, each of these methods has defects that

have been described in detail by Rezaei and others [3]. Due to these restrictions and simplicity of the analytical modeling, a new theoretical energy-based model with further incorporated effective parameters is suggested in this work to evaluate the combined height of caving and fracturing zones above the longwall gobs. Here, a combination of the height of caving and fracturing zones is considered as the height of destressed zone (HDZ). Beyond this height, the overburden pressure will be transferred towards the adjacent solid sections. Therefore, HDZ has a vital role in the amount of transferrable loads to the front abutment, adjacent access tunnels, pillars, and panel rib-sides. Thus to suitably evaluate the amount of transferrable loads to the adjacent gates and the intervening pillars, the amount of HDZ must be estimated [3]. In addition, evaluating the induced ground subsidence is a critical topic in longwall mining, which is affected by the caving and fracturing of the roof rock strata [8]. Actually, the complete/total value of HDZ can be achieved while the caved material system would be stable. On the other hand, the ground subsidence phenomenon will be stopped by stabilization of the caved material system. Therefore, the stability time of the caved material system is very important in determination of maximum HDZ and ground surface subsidence due to longwall mining.

The main aim of this work was to investigate HDZ above the longwall gobs in long-term conditions, and to estimate the stability time of the caved material system. For this purpose, the time-dependent analytical determination of HDZ is firstly described. Then the stability time of the caved material system is calculated based upon the principle of minimum potential energy. Unlike the past studies, the geometrical and geomechanical properties of roof rock strata as well as the pressure, time, and temperature-dependent parameters of the caved materials were considered in the HDZ prediction simultaneously. Finally, the effects of time and temperature-related parameters on HDZ and the stability time of the caved material systems were evaluated.

2. Background

2.1. Distributed zones above mined panel

After coal extraction in longwall mining, the roof rock strata are allowed to be fractured and caved in the mined area (called the goaf area). This process causes disturbance of the original in-situ stress regime and the hydraulic conductivity. By progressive in extraction, the fracturing and caving phenomena of roof strata gradually extend upwards and will cause the disturbed roof strata to become destressed. Prediction of HDZ above the longwall gobs plays an important role in determining the transferred loads towards the front abutments and panel rib-sides in which the gates and pillars are situated. For this purpose, many researchers have investigated the behavior of working roof, process of gradual upward movement, and determination of the height of caving and fracturing zones. These issues have recently been discussed by some investigators [1-3], in which the previous related investigations have also been referred. According to these, three zones of disturbance have been identified above the mined panel (Figure 1). These zones include the caved, fractured, and continuous deformation zones [9]. As it can be seen in Figure 1, these zone can reach 20, 20-50, and more than 50 times the extracted seam thickness (mining height), respectively. However, extension of each zone depends on the geological and geomechanical conditions of overburden strata including the strength properties of rocks, in-situ stress, thickness of seam (rock) and overburden, and type and nature of the strata [10].

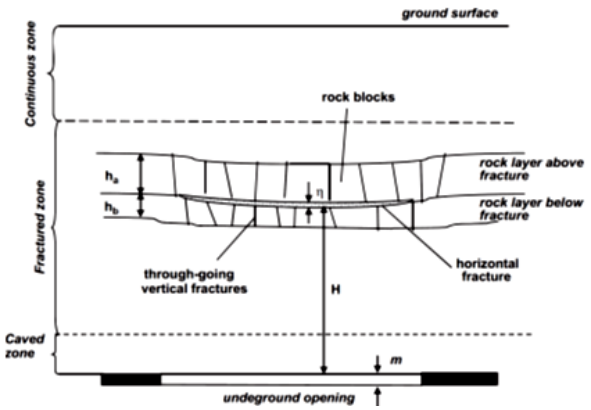

Figure 1. Three movement zones in overburden due to longwall mining [10].

2.2. Literature review

Comprehensive literature review about the disturbed zones over the goaf area was conducted in detail [2, 3, 6, 7]. However, for brevity, only the most important and related ones of the older studies were reviewed. Instead, the new investigations in the field of roof rock failure strata and its relationship with the ground surface subsidence are discussed in more detail. Roof rock behaviour above the goaf area was studied by Eavenson [11] for the first time. He believed that the inner-burden shear failure during multiple seam extraction in longwall mining extended to the ground surface. However, Denkhaus [12] proved that the maximum HDZ would be equal to 50% and 63% of the depth of cover above the panel for rocks with sufficient and insufficient cohesion, respectively. Some other researchers have proposed different models to calculate the heights of caved and fractured/destressed zones above the goaf area in terms of the coefficient of extracted coal seam thickness or mining height. For example, Ropski and Lama [13] have shown that the primary and secondary caving zones extend to a height of 3-3·5 times the extracted coal seam thickness. Palchik [14] believed that the thickness of the fractured zone varied from 20 to 100 times the extracted seam thickness. Palchik [15] has found that the maximum heights of interconnected fractures and separate horizontal fracture zones reach 19-41 and 53-92 times the extracted coal seam thickness, respectively. According to Zhimin and others [16], the height of the fractured zone was obtained to be 14.33–17.71 and 16.04 times the mining thickness from in-situ measurements and numerical modeling, respectively. Zhang and others [17] have investigated the overburden fracture evolution laws in mining a very thick coal seam under water-rich roof using the numerical modeling. Their finding proved that the height of the fractured zone in the overburden strata ranged from 18.66 to 47.66 times the extraction seam height. Gao and others [18] have developed a numerical approach to simulate the progressive caving of strata above a longwall panel. Their results show that the fractures extend approximately 40 m into the roof.

In addition to the above reviewed references, the newly related research works that have been conducted in the latest recent years (2015, 2016, and 2017) are examined here in detail. The horizontal displacement distribution caused by a single advancing longwall panel excavation has been evaluated by Tajduś [19]. He assumed that the value of the horizontal displacement was proportional to the slope of subsidence value. Xue and others [20] have analyzed the movement and fracture of overlying strata based on the experimental analysis. They concluded that the maximum height of caving, fracturing, and bending zones were equal to 7.5, 25, and 25 times the mining height, respectively. Based on the in-situ measurement and numerical and theoretical modeling, Bai and others [21] have studied the roof deformation and failure characteristics in advancing longwall working face, and proposed a dynamic mechanical model of the roof structure. Ming-he and others [22] have developed a numerical model to evaluate the stress distribution around the longwall face based on the caving height zone. The research conclusion has highlighted that the height of caving zone is the main parameter effective on the coefficient of stress concentration around the longwall panel. The in-situ measurements performed by Palchik [23] showed that the maximum height of caved zone could reach 20 times the mining height. According to a conceptual model proposed by Qu and others [24], the maximum relative height of key stratum is about 20.7 times the extracted seam thickness.

According to a coalface failure model proposed by Jiachen and others [25], due to longwall panel extraction, the height of caving zone increases with increase in the mining height. According to Meng and others [26], the ratios of the average caving-fracturing zone height to the extracted coal seam thickness in the Daliuta coal mine from the in-situ tests, physical modeling, and numerical simulation are equal to 20.3, 22.8, and 19.4, respectively. Theoretical evaluation of the abutment pressure in longwall coal mining conducted by Zhu and others [27] based on the analysis of load transfer mechanisms of key stratum (KS) showed the importance of roof rock strata disturbed zone in transferred load to the sides and front abutments. Yu and others [28] have evaluated the stress changes and deformation of coal pillars and gateroads affected by the mining-induced stress based on the in-situ measurements. Accordingly, they have concluded that the adjacent panel extraction plays a crucial role in the main deformation and damage of the surrounding gate roads. Xie and Xu [29] have studied the key stratum above the mined panel, and evaluated its effect on the mining abutment pressure of a coal seam. They proved that the abutment pressure of the field model with a key stratum was 42% higher than that of the model

without any key stratum. Rezaei [6] has developed a new neural network model for estimation of the height of caving–fracturing zone over the longwall gobs and evaluation of the effect of geomechanical parameters on this height. Rezaei and others [7] have proposed an optimum ANN model to determine HDZ over the mined panel in longwall mining. Beside the determination of disturbed zones above the mined panel, the relationship between the ground subsidence and overburden failure and also time-dependent failure and deformation of roof strata time have been investigated by some researchers [30-34]. These showed that numerous factors affected the ground subsidence due to mining operation including the mining method, mining depth, ore thickness, stope size, dip angle of ore body, geological structure, nature of overburden and water contents, roof supports, etc. [34]. However, there is no formulated analytical basis to show the relation between the ground subsidence and disturbed zones above the mined panel in log-term condition.

Considering the above literature review, it is obvious that there are various in-situ measurements, empirical, mathematical, numerical, and physical models to predict the height of disturbing zones above the longwall gobs. In all the previous investigations, the effects of time- and temperature-related parameters were ignored in the evaluation of the height of caving and fracturing zones. To overcome these shortages, a time-dependent energy model for evaluation of HDZ above the longwall gobs is described in the current study. Furthermore, the stability of the caved material system is discussed for subsidence estimation subjects. The main application of the estimation of the caved material system stability time is in the prediction of maximum occurred ground subsidence in surface due to longwall mining. It is obvious that the ground subsidence would be stable while the caved material system is stable. Indeed, determination of the time stability of the caved material system helps the ground subsidence occurrence period determination. Knowledge of the maximum surface subsidence and it occurrence period helps engineers in designing the preventive supports and supply the safety requirements.

3. Stability analysis model

3.1. Time-dependent calculation of HDZ

Energy consideration in longwall mining, and consequently, determination of HDZ above the longwall panel in long-term and short-term conditions have already been discussed by Rezaei and others [3-5]. However, HDZ in the long-term condition was calculated by Rezaei and others [5] recalled here in order to develop a new procedure for evaluation of the stability time of the caved material system as well as estimation of the effect of time- and temperature-related parameters on HDZ. According to Rezaei and others [3], coal seam extraction in longwall mining causes disturbance of the energy balance within a system enclosing mine openings and surrounding rocks. This leads to release the stored strain energy in the mined seam. However, this released energy will not be lost according to the principle of energy survival but transfer from one equilibrium state to another. Indeed, the released energy is consumed in the fracturing, caving, and destressing of the over roof rock layers. Accordingly, it is concluded that the total stored strain energy in the mined seam (U_m) is equal to the strain energy stored in the roof destressed zone (U_d), as shown in the following equation:

$$\mathrm{U_m = U_d} \tag{1}$$

By the assumption that there exist no permanent supports in longwall mining, i.e. ignoring the effect of body forces, here, the total stored strain energy in the mined seam (U_m) is calculated by the Salamon [35] equation, as follows:

$$U_m = \frac{1}{2}\int_{S_m} T_i^{(p)} u_i^{(p)} dS \tag{2}$$

where T_i^p, u_i^p, and S_m are the stress or traction vector acting on a surface, and the component of the displacement vector before starting the mining and mined layer area, respectively. These parameters are computed as follow [35]:

$$\mathrm{T_i^{(p)} = \sigma_v = \gamma H}$$
$$\mathrm{u_i^{(p)} = \frac{(1+\nu)(1-2\nu)\gamma H^2}{2(1-\nu)E}} \tag{3}$$

where σ_v, E, γ, H, and ν are the initial stress due to the overburden pressure, rock mass elastic modulus, rock mass unit weight, depth of cove, and rock mass Poisson ratio, respectively.

Substitution of Eq. (3) into Eq. (2) leads to:

$$U_m = \frac{(1+\nu)(1-2\nu)\gamma^2 H}{2(1-\nu)E}\int_{S_m} H^2 dA \tag{4}$$

In Eq. (4), the integral term is the moment of inertia of surface S_m with respect to the plane of ground surface. Thus according to the parallel-axis theorem in statics:

$$I = \int_{S_m} H^2 dA = I_0 + A_m D^2 \quad (5)$$

where I_0 is the moment of inertia of the mined area (panel) cross-section with respect to a horizontal line across its centre of gravity, A_m is the cross-section of the mined panel, H is the depth of cove, and D is the vertical distance from the panel centre of gravity to the ground surface. With regard to the rectangular cross-section of the mined panel, A_m, I_0, and D are calculated as follow:

$$\begin{aligned} A_m &= L_w \times h_s \\ I_0 &= \frac{L_w h_s^3}{12} \\ D &= H + h_s / 2 \end{aligned} \quad (6)$$

where L_w and h_s are the panel width and extracted coal seam thickness, respectively.
When Eqs. (5) and (6) are substituted into Eq. (4), the final equation of the total stored energy in the extracted coal seam is obtained:

$$U_m = \frac{(1+\nu)(1-2\nu)\gamma A_m \sigma_v}{2(1-\nu)E}\left(\frac{h_s^2}{3} + H^2 + Hh_s\right) \quad (7)$$

The strain energy stored in the roof destressed zone (U_d) is generally composed of elastic strain energy (U_E) and viscoplastic strain energy (U_V).

$$U_d = U_E + U_V \quad (8)$$

The non-linear rheological constitutive model introduced by Zhang and others [36] is utilized to investigate the rheological properties of the caved materials and calculate the components of U_d. In this model, the elastic modulus (E), coefficient of viscosity (μ), and threshold value of stress (σ_s) are considered based upon the modified Bingham model [36]. According to this model, the stress of caved materials before and after the yield point (threshold value of stress) is calculated as follows:

$$\begin{cases} \sigma = E_0 e^{-at}\varepsilon & \sigma \le \sigma_s \\ \sigma = \dfrac{\varepsilon}{K} - \lambda\varepsilon, & \sigma > \sigma_s \end{cases} \quad (9)$$

where E_0 is the initial elastic modulus, a is the material constant, t is the pressure time of caved materials, ε is the strain of caved materials, λ is the slope of material hardening stage, and K is the coefficient that is calculated by the following equation:

$$K = \frac{1}{E_0 e^{-at}} + \frac{Bt^{\alpha}}{\sigma_s^{\mu}} \quad (10)$$

where $B = 1/\eta_0 C\alpha$; η_0 is the initial coefficient of viscosity; and C, μ, and α are the material constants related to temperature.
To calculate the elastic strain energy of the caved materials within the destressed zone (U_E), the common equation of strain energy is used. If the destressed zone above the longwall panel is considered as a separate system, its absorbed elastic strain energy can be calculated as follows:

$$U_E = \frac{1}{2}\int \sigma\varepsilon dV = \frac{1}{2}\int_0^h \sigma\varepsilon A dh \quad (11)$$

where σ is the applied stress on the caved materials, ε is the strain occurring under the applied stress, h is the height of the caved materials within the destressed zone, and A is the unit surface of the system. Here, A_d is considered as the unit surface of the destressed zone, which is equal to the panel width multiplied by the unit length of longwall panel ($A_d = L_w \times 1^m$). After completion of the caving process, the caved materials are thoroughly compressed, and then the total height of caved materials is equivalent to HDZ ($h = H_d$). Thus Eq. (11) can be modified to:

$$U_E = \frac{1}{2}\sigma\varepsilon A_d H_d \quad (12)$$

In Eq. (9), the caved material system has the elastic and viscoplastic properties when $\sigma \le \sigma_s$ and $\sigma \ge \sigma_s$, respectively. Accordingly, the elastic and viscoplastic components of strain energy are calculated based on its related stress in this equation. Therefore, substitution of the elastic and viscoplastic parts of Eq. (9) into Eq. (12) lead to calculate the elastic strain energy (U_E) and viscoplastic strain energy (U_V) stored in the roof destressed zone, as follow:

$$U_E = \frac{1}{2} E e^{-at} A_d H_d \varepsilon^2 \quad (13)$$

$$U_V = \left(\frac{\varepsilon^2}{2K} - \frac{\lambda\varepsilon^2}{2}\right) A_d H_d \quad (14)$$

Instead of the strain of caved materials, this equation can be instituted; it was developed by Salamon [37] to describe the stress-strain behavior of caved materials:

$$\varepsilon = \frac{\sigma_c}{[E + \frac{\sigma_c}{\varepsilon_m}]} \quad (15)$$

where σ_c is the uniaxial compressive strength of caved materials and ε_m is the maximum possible strain of the caved materials. ε_m depends on the bulking factor (b), and can be determined using the following equation [38]:

$$\varepsilon_m = \frac{b-1}{b} \quad (16)$$

By substituting Eqs. (15) and (16), Eqs. (13) and (14) could be modified as follow:

$$U_E = \frac{Ee^{-at} A_d H_d \sigma_c^2}{2[E + \frac{b\sigma_c}{(b-1)}]^2} \quad (17)$$

$$U_V = \frac{A_d H_d \sigma_c^2}{2[E + \frac{b\sigma_c}{(b-1)}]^2} [Ee^{-at} + \frac{\sigma_s^\mu}{Bt^\alpha} - \lambda] \quad (18)$$

Now the total strain energy stored in the roof destressed zone (U_d) is achieved by substituting Eqs. (17) and (18) into Eq. (8) in the following form:

$$U_d = \frac{A_d H_d \sigma_c^2}{2[E + \frac{b\sigma_c}{(b-1)}]^2} [2Ee^{-at} + \frac{\sigma_s^\mu}{Bt^\alpha} - \lambda] \quad (19)$$

Finally, if Eqs. (19) and (7) are substituted into Eq. (1), HDZ in time-dependent condition is calculated as follows:

$$H_d = \frac{\frac{(1+\nu)(1-2\nu)\gamma A_m \sigma_v}{(1-\nu)E}\left[\frac{h_s^2}{3} + H^2 + Hh_s\right]}{\frac{A_d \sigma_c^2}{[E + \frac{b\sigma_c}{(b-1)}]^2}[2Ee^{-at} + \frac{\sigma_s^\mu}{Bt^\alpha} - \lambda]} \quad (20)$$

3.2. Stability time of goaf

Estimation of stability time of the caved material systems is very important to determine the maximum surface subsidence due to longwall mining. In this research work, stability analysis of the proposed time-dependent energy model is conducted based on the principle of minimum potential energy of the caved materials system. It is obvious that the total potential energy of the caved material structure (Π) is composed of strain energy (U_d) and external work (W):

$$\prod = U_d - W \quad (21)$$

The total strain energy stored in the roof destressed zone (U_d) was calculated in the previous section, as shown in Eq. (19). Thus only the external work (W) is calculated in this section. Assuming that P is the pressure of roof rocks and u is the deformation of caved materials, the external work of roof rocks upon the caved materials (W) can be written as:

$$W = pu \quad (22)$$

Here, the deformation parameter (u) is selected as the state variable. For matching the external work and strain energy equations, the stress (σ_c) existing in Eq. (19) must be written in terms of deformation. To do so, stress and strain can be defined according to the stress-strain behaviour of caved materials in rheological constitutive model by Zhang and others [36], as the following equations:

$$\sigma = \varepsilon / K \quad (23)$$

$$\varepsilon = u / h \quad (24)$$

Given that the discussed height in this study is the height of destressed zone in long-term condition (H_d), we can write:

$$\varepsilon = u / H_d \quad (25)$$

Replacing Eq. (25) into Eq. (23) leads to:

$$\sigma_c = \frac{u}{H_d K} \quad (26)$$

Substitution of Eq. (26) into the stress parameter of Eq. (19) leads to:

$$U_d = \frac{A_d u^2}{2H_d K^2 [E + \frac{bu}{H_d K(b-1)}]^2} [Ee^{-at} + \frac{1}{K} - \lambda] \quad (27)$$

When Eqs. (27) and (22) are substituted into Eq. (21), the total energy of structure (Π) is achieved as follows:

$$\Pi = \frac{A_d u^2}{2H_d K^2 [E + \frac{bu}{H_d K(b-1)}]^2} [Ee^{-at} + \frac{1}{K} - \lambda] - pu \quad (28)$$

According to the principle of minimum potential energy, the system is stable when the energy of the system reaches a minimum. If $\delta^2 \Pi \geq 0$ and $\delta \Pi = 0$, the energy of the system reaches a minimum

(δ is the derivative sign). In the case of $\delta^2\Pi < 0$ and $\delta\Pi \neq 0$, the energy of the system cannot reach a minimum. These concepts are used in order to calculate the stability time of the caved material system in longwall mining. Accordingly, the second derivative of total energy of structure (Π) or Eq. (28) is achieved as:

$$\delta^2 \prod = \frac{A_d}{H_d K^2 E^2}[Ee^{-at} + \frac{1}{K} - \lambda] \times (\partial u)^2 \quad (29)$$

In our investigation, the state of transition from the instability to stability ($\delta^2\Pi = 0$) is considered as the stability time of the caved materials system. Therefore, the time of stability of caved material system can be obtained when $\delta^2\Pi = 0$. Since K > 0 in Eq. (29), we can write:

$$KEe^{-at} + 1 - K\lambda = 0 \quad (30)$$

Substitution of Eq. (10) into Eq. (29) and rearranging it lead to:

$$2\sigma_s^{\mu} Ee^{-at} + (Ee^{-at})^2 Bt^{\alpha} + \lambda Bt^{\alpha} Ee^{-at} = \lambda\sigma_s^{\mu} \quad (31)$$

To solve Eq. (31) and obtain the stability time of the caved material structure, a graphical method can be used. For this purpose, Eq. (31) is divided into two functions, as follows:

$$f(t) = 2\sigma_s^{\mu} Ee^{-at} + (Ee^{-at})^2 Bt^{\alpha} + \lambda Bt^{\alpha} Ee^{-at} \quad (32)$$

$$g(t) = \lambda\sigma_s^{\mu} \quad (33)$$

The intersection of the graphs of the above two equations will be the stability time of the caved material structure (t_s). Actually, these two graphs and their intersection value could be applied to obtain the stability time of caved materials that practically outlined in the following sub-section.

3.3. Validation of proposed model

In order to validate the proposed model, the particular experimental data was utilized to plot the graphs of the above-mentioned two functions (given in Eqs. (32) and (33)) and obtain the corresponding stability time. As an engineering example, the values of the measured experimental data conducted by Zhang and others [36] were applied for drawing the graphs and calculation of the stability time of the caved material structure (t_s). These measured experimental datasets are presented in Table 1. Also the geometrical and geomechanical parameters are kept constant according to the in-situ measurements conducted by RafiqulIslam and others [39], as shown in Table 2. On the basis of the experimental data given in Table 1, Zhang and others [36] have calculated the stability time of the caved materials using the analytical model and compared the results obtained with the observations in practice. Therefore, the results of the proposed model in this research work can be compared with the result of the above research work as a comparison basis for the validation aim. Considering this data, the graphs of *f(t)* and *g(t)* were plotted and shown in Figure 2. According to this figure, the stability time of the caved material structure is equal to 1.643 years. Thus from the first caving period until 1.643 years later, the caved material system is unstable and HDZ increases consequently. After this time, the system will be stable, and the additional subsidence will not occur in the ground surface. The stability time calculated by Zhang and others [36] was 1.51 years. As it can be seen from this comparison, the results of the current research work are in a good agreement with the results obtained by Zhang and others [36], which conforms well to the observations in practice. Thus it can be concluded that the proposed model can be successfully applied for the long-term stability analysis of goaf area and calculation of the stability time of the caved materials. Moreover, this model and its corresponding computed stability time can be linked to the maximum ground surface subsidence calculation in the future research works.

Table 1. Experimental parameters used in plotting graphs [36].

σ_s (MPa)	E (MPa)	B	μ	α	λ	a
20	59	1.24	2	0.3	3	1

Table 2. Geometrical and geomechanical parameters and corresponding mean caving and fracturing zone used in current study calculations [39].

H (m)	L_w (m)	γ (KN/m^3)	E (GPa)	ν	σ_c (MPa)	b	h_s (m)	HDZ (m)
290	120	2.7	3.5	0.22	50	1.5	3.5	29.5

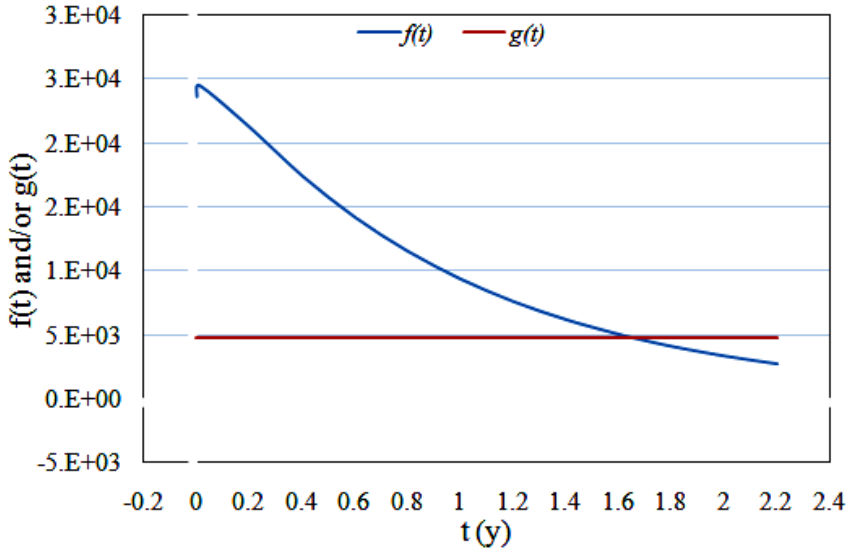

Figure 2. Graphs of *f(t)* and *g(t)* to obtain stability time of caved material structure.

4. Parametric study

Beside the geometrical and geomechanical parameters, the time and temperature parameters are also the most important variables, and are very crucial in the stability analysis of the goaf area. Knowledge of the height of the caved, fractured, and destressed zone along with the sustainability of the goaf area is very crucial during the time and extraction phases. Also compression of the caved material causes increase in temperature, which affects the bulking and compaction characteristics of the caved material. These may affect the instability of the caved material system and other related objects, i.e. roof failure and ground subsidence. Despite this great importance, this issue was rarely investigated by previous researchers. Thus the effects of pressure and time of caved materials and temperature-related parameters are discussed in detail here. Accordingly, variations in HDZ versus material constant (a), slope of materials hardening stage (λ), temperature-related parameters of α, C, and μ, threshold value of stress (σ_s), initial coefficient of viscosity (η_0), and pressure time of caved materials (t) are shown in Figures 3-10, respectively. In these figures, the relative influence of each parameter on HDZ is identified by varying the desired parameter and maintaining fixed values for the other parameters according to Table 1.

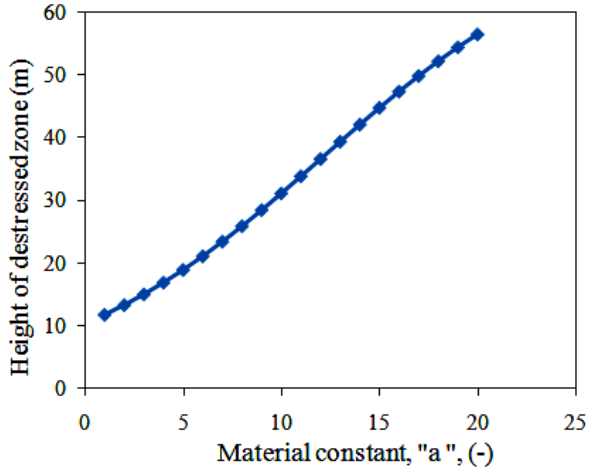

Figure 3. Relationship between HDZ and material constant.

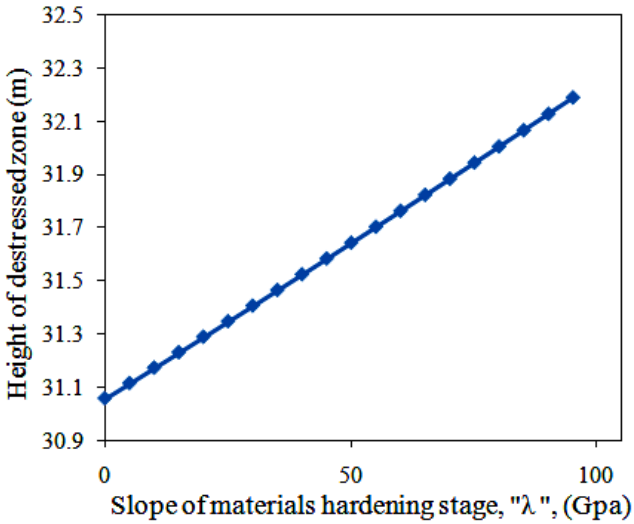

Figure 4. Relationship between HDZ and slope of material hardening.

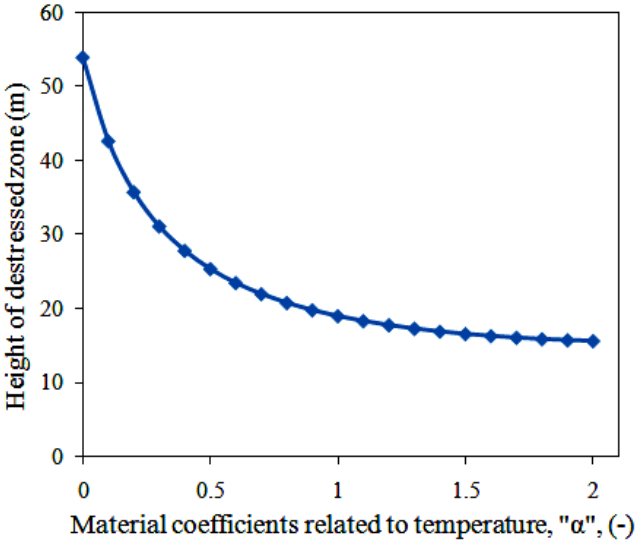

Figure 5. Relationship between HDZ and temperature-related parameter (α).

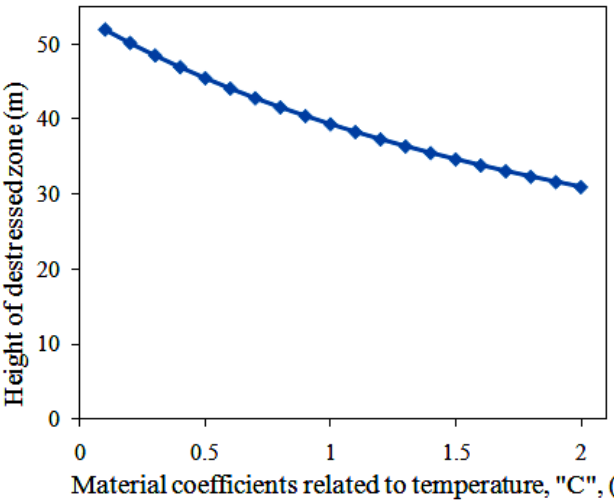

Figure 6. Relationship between HDZ and temperature-related parameter (C).

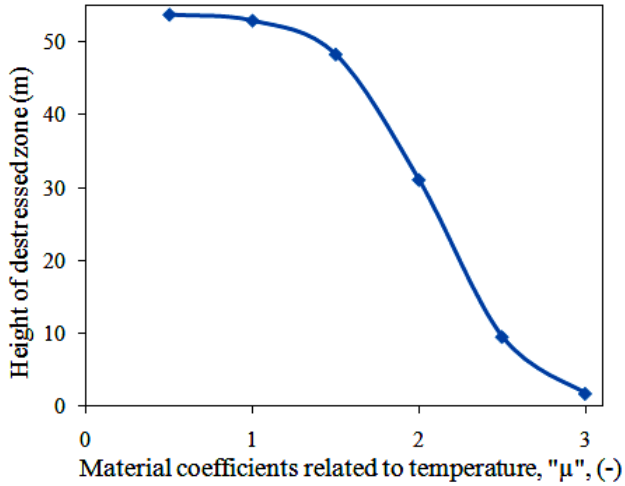

Figure 7. Relationship between HDZ and temperature-related parameter (μ).

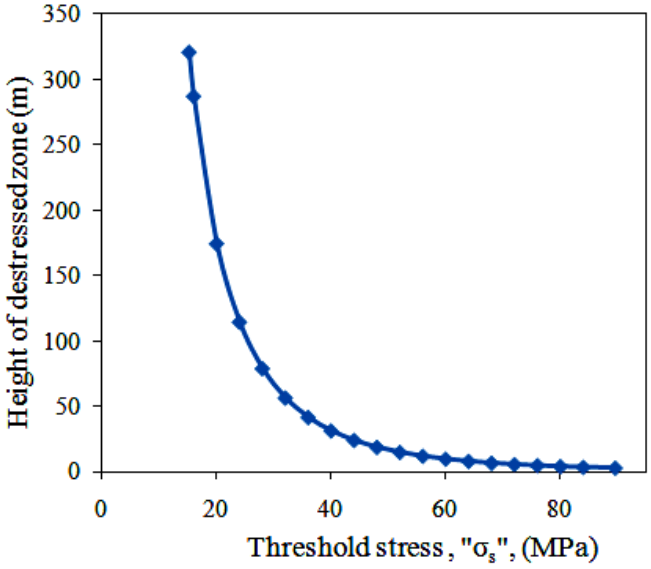

Figure 8. Relationship between HDZ and threshold value of stress.

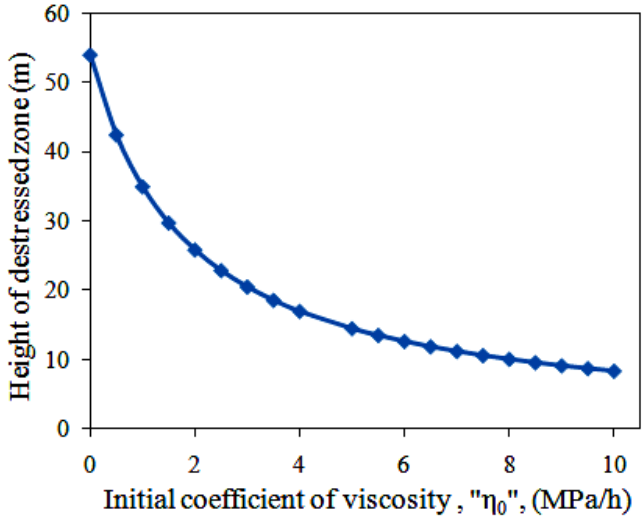

Figure 9. Relationship between HDZ and initial coefficient of viscosity.

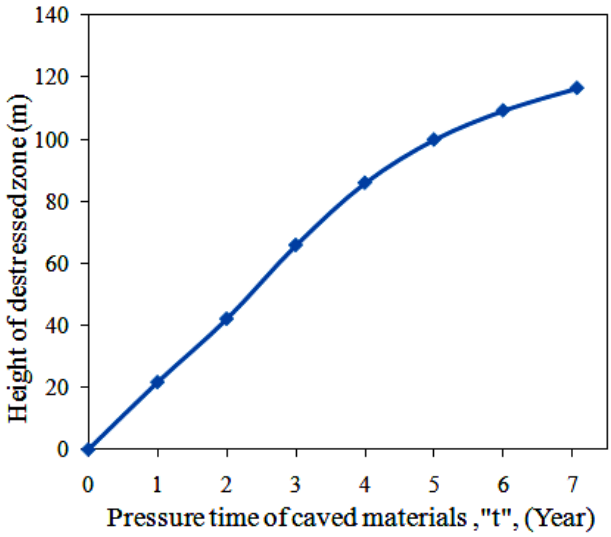

Figure 10. Relationship between HDZ and pressure time of caved materials.

According to Figure 3, the material constant has a direct relation with HDZ. Indeed, the material constant (a) is a positive material constant, named the softening parameter that describes the softening characteristic of the material or rocks. If the softening parameter of caved material increases, the compression capacity of the material will increase. Therefore, with increase in the material constant, more compression will occur, and then further roof caving will take place. As it can be seen in Figure 4, when the slope of material hardening increases, HDZ increases by a linear relation. It is obvious that the higher value of slope of material hardening means that the caved materials have a more compression capability. This causes an additional caving, and thus a further value of HDZ. Figures 5-7 indicate that the temperature-related parameters including α, C, and μ are in non-linear inverse relations with HDZ. It is known that increasing the temperature and its related parameters increases the amount of fluid, and lowers the strain rate of the caved material. Decreasing the strain rate lowers the compaction of the caved material, and thus decreases the caving process of the roof rock strata. Thus HDZ will increase with increase in the temperature-related parameters including α, C, and μ. As it can be seen in Figure 8, a higher value for threshold stress leads to a lower HDZ. The threshold value of stress normally depends on the compressive strength of caved materials. Obviously, materials with high compressive and threshold stress values have fewer tendencies to cave, and as a result, HDZ will decrease. It can be concluded from Figure 9 that the higher the initial coefficient of viscosity, the lower is HDZ. This proves the fact that if the coefficient of viscosity of caved rocks increases, less compression of them will occur. Thus the amount of roof caving decreases, and thus HDZ will be less. Finally, Figure 10 demonstrates that HDZ has a direct relation with the pressure time of caved materials. It is clear that over the time, the caved material will be further compressed, and therefore, enough space will be provided for more caving. As a result, the height of the destressed zone increases over the time. In addition, the semi-fractured or suspended rocks will cave over the time that causes the increase in HDZ.

As a general conclusion of the parametric study, it can be concluded that the time and temperature-related parameters considerably affect HDZ (see Figures 5-7 and 10). This issue has been neglected in the previous research works, which can influence the estimated HDZ and other related variables, especially in time-dependent situations. Therefore, the proposed model could be preferred in long-term conditions.

5. Sensitivity analysis

In this section, sensitivity analysis is conducted to estimate the most and least effective parameters on HDZ among the time- and temperature-related parameters. Sensitivity analysis could be performed in two different ways, i.e. novel and traditional procedures. In novel procedures, available equations and techniques such as cosine amplitude method [40-42] could be applied for this purpose. However, in the traditional methods, the influence of an input variable on the corresponding output could be achieved by systematic changing of it and keeping fixed values for the other inputs of the model. The latest procedure was used in this work for the sensitivity

objects. To do so, to achieve the influence of each parameter on HDZ, other parameters were assumed constant, according to the experimental values given in Table 1 in the first stage. Then the value of the considered input changed systematically from -30% to +30% (i.e. three values) of its actual value in Table 1 and corresponding HDZ calculated. This process was performed for all of the time and temperature-related parameters, and the graphs obtained along with their gradients are demonstrated in Figure 11. The graph with higher gradient shows a more impact of its corresponding input on the output. As it can be seen in Figure 11, temperature-related parameters (α and μ), material constant (a), and time (t) are the most effective variables on the HDZ, while the slope of material hardening (λ) is the least effective one on it.

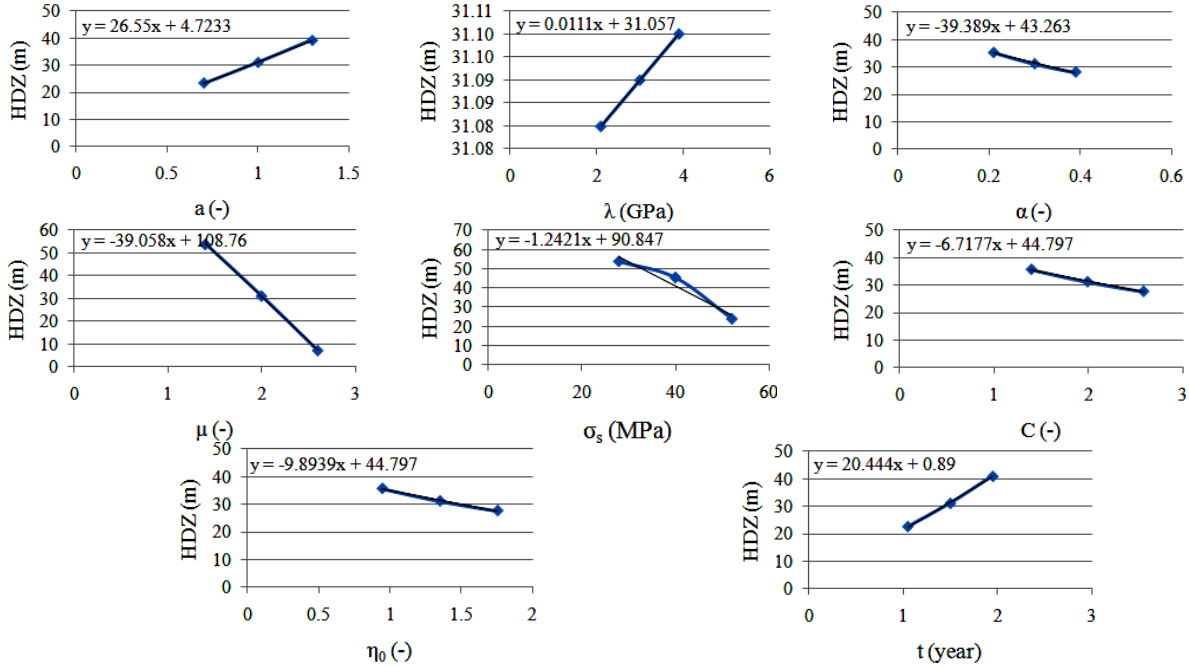

Figure 11. Sensitivity analysis results of time- and temperature-related parameters.

6. Conclusions

A new analytical model was developed in this research work for the stability analysis of the longwall goaf area. To do so, a time-independent model was developed for the height of destressed zone (HDZ) above the mined panel. Then the stability time of the caved material system in longwall mining was analyzed based upon the principle of minimum potential energy. Eventually, the parametric study and sensitivity analysis were performed in order to evaluate the relation of time- and temperature-related parameters with HDZ, and determine the effective parameters. The results obtained showed that the material constant, slope of material hardening stage, and pressure time of caved materials have direct influences on HDZ. On the other hand, the temperature-related parameters (α, C, and μ), threshold stress, and initial coefficient of viscosity have inverse influences on HDZ. Moreover, temperature-related parameters, i.e. α and μ, material constant, and time are the most effective parameters on HDZ, and the slope of material hardening is the least effective one. As seen, time- and temperature-dependent parameters have significant effects on HDZ and should not be neglected in the modeling. A general consequence of the new proposed analytical model compared to the previous ones is that it incorporates the effects of pressure time and temperature-related parameters of caved materials on HDZ along with the estimation of the stability time of the goaf. The long-term evaluation of HDZ time plays an important role in an accurate estimation of transferred loads towards the gates and pillars during the anytime of mining operation lifetime. In addition, prediction of the stability time of caved materials helps the exact determination of maximum ground surface subsidence due to longwall mining. However, these topic points require further investigations and validation and recommendations for future works.

References

[1]. Majdi, A., Hassani, F.P. and Yousef Nasiri, M. (2012). Prediction of the height of destressed zone

above the mined panel roof in longwall coal mining. International Journal of Coal Geology. 62: 62-72.

[2]. Majdi, A. and Rezaei, M. (2013). Application of artificial neural networks for predicting the height of destressed zone above the mined panel in longwall coal mining. 47th U.S. Rock Mechanics/Geomechanics Symposium. San Francisco. California. USA. pp. 1665-1673.

[3]. Rezaei, M., Hossaini, M.F. and Majdi, A. (2015). A time-independent energy model to determine the height of destressed zone above the mined panel in longwall coal mining. Tunnelling and Underground Space Technology. 47: 81-92.

[4]. Rezaei, M., Hossaini, M.F. and Majdi, A. (2015). Determination of longwall mining-induced stress using the strain energy method. Rock Mechanics and Rock Engineering. 48: 2421-2433.

[5]. Rezaei, M., Hossaini, M.F. and Majdi, A. (2015). Development of a time-dependent energy model to calculate the mining-induced stress over gates and pillars. Journal of Rock Mechanics and Geotechnical Engineering. 7: 306-317.

[6]. Rezaei, M. (2016). Development of an intelligent model to estimate the height of caving-fracturing zone over the longwall gobs. Neural Computing & Applications. doi: 10.1007/s00521-016-2809-3.

[7]. Rezaei, M., Farouq Hossaini, M., Majdi, A. and Najmoddini, I. (2017). Determination of the height of destressed zone above the mined panel: An ANN model. International Journal of Mining and Geo-Engineering. 51 (1): 1-7.

[8]. Ghabraie, B., Ghabraie, K., Ren, G. and Smith, J. (2017). Numerical modelling of multistage caving processes: insights from multi-seam longwall mining-induced subsidence. International Journal for Numerical and Analytical Methods in Geomechanics. 41: 959-975.

[9]. Chekan, G.J. and Listak, J.M. (1993). Design practices for multiple-seam longwall mines. Information circular/1993 (No. PB-94-113545/XAB; BUMINES-IC-9360). Bureau of Mines. Pittsburgh. PA (United States). Pittsburgh Research Center.

[10]. Palchik, V. (2010). Experimental investigation of apertures of mining-induced horizontal fractures. International Journal of Rock Mechanics & Mining Sciences. 47: 502-508.

[11]. Eavenson, H. (1923). Mining an upper bituminous seam after a lower seam has been extracted. Transaction of AIME. 69: 398-405.

[12]. Denkhaus, H.G. (1964). Critical review of strata movement theories and their application to practical problems. Journal of the Southern African Institute of Mining and Metallurgy. 64 (8): 310-332.

[13]. Ropski, S.T. and Lama, R.D. (1973). Subsidence in the near-vicinity of a longwall face. International Journal of Rock Mechanics and Mining Sciences abstract. 10 (2): 105-106.

[14]. Palchik, V. (1989). Analytical and empirical prognosis of rock foliation in rock masses. Journal of Coal Ukraine. 7: 45-46.

[15]. Palchik, V. (2003). Formation of fractured zones in overburden due to longwall mining. Journal of Environmental Geology. 44 (1): 28-38.

[16]. Zhimin, X., Yajun, S., Qinghong, D., Guowei, Z. and Shi, L. (2010). Predicting the height of water-flow fractured zone during coal mining under the Xiaolangdi Reservoir. Mining Science and Technology. 20: 434-438.

[17]. Zhang, Y., Tu, S., Bai, Q. and Li, J. (2013). Overburden fracture evolution laws and water-controlling technologies in mining very thick coal seam under water-rich roof. International Journal of Mining Science and Technology. 23 (5): 693-700.

[18]. Gao, F., Stead, D. and Coggan, J. (2014). Evaluation of coal longwall caving characteristics using an innovative UDEC Trigon approach. Computers and Geotechnics. 55: 448-460.

[19]. Tajduś, K. (2015). Analysis of horizontal displacement distribution caused by single advancing longwall panel excavation. Journal of Rock Mechanics and Geotechnical Engineering. 7: 395-403.

[20]. Xue, J., Wang, H., Zhou, W., Ren, B., Duan, C. and Deng, D. (2015). Experimental research on overlying strata movement and fracture evolution in pillarless stress-relief mining. International Journal of Coal Science & Technology. 2: 38-45.

[21]. Bai, J.B., Shen, W.L., Guo, G.L., Wang, X.Y. and Yu, Y. (2015). Roof deformation, failure characteristics, and preventive techniques of gob-side entry driving heading adjacent to the advancing working face. Rock Mechanics and Rock Engineering. 48: 2447-2458.

[22]. Ju, M.H., Li, X.H., Yao, Q.L., Li, D.W., Chong, Z.H. and Zhou, J. (2015). Numerical investigation into effect of rear barrier pillar on stress distribution around a longwall face. Journal of Central South University. 22 (11): 4372-4384.

[23]. Palchik, V. (2015). Bulking factors and extents of caved zones in weathered overburden of shallow abandoned underground workings. International Journal of Rock Mechanics & Mining Sciences. 79: 227-240.

[24]. Qu, Q., Xu, J., Wu, R., Qin, W. and Hu, G. (2015). Three-zone characterisation of coupled strata and gas behaviour in multi-seam mining. International Journal of Rock Mechanics & Mining Sciences. 78: 91-98.

[25]. Jiachen, W., Shengli, Y. and Dezhong, K. (2016). Failure mechanism and control technology of longwall coalface in large-cutting-height mining method. International Journal of Mining Science and Technology. 26: 111-118.

[26]. Meng, Z., Shi, X. and Li, G. (2016). Deformation, failure and permeability of coal-bearing strata during longwall mining. Engineering Geology. 208: 69-80.

[27]. Zhu, S., Yu, F. and Jiang, F. (2016). Determination of abutment pressure in coal mines with extremely thick alluvium stratum: a typical kind of rockburst mines in china. Rock Mechanics and Rock Engineering. 49: 1943-1952.

[28]. Yu, B., Zhang Z., Kuang, T. and Liu, J. (2016). Stress changes and deformation monitoring of longwall coal pillars located in weak ground. Rock Mechanics and Rock Engineering. 49: 3293-3305.

[29]. Xie, J.L. and Xu, J.L. (2017). Effect of key stratum on the mining abutment pressure of a coal seam. Geosciences Journal. 21: 267-276.

[30]. Xiao, W., Hu, Z., Chugh, Y.P. and Zhao, Y. (2014). Dynamic subsidence simulation and topsoil removal strategy in high groundwater table and underground coal mining area: a case study in Shandong Province. International Journal of Mining, Reclamation and Environment. 28: 250-263.

[31]. Villegas, T. and Nordlund, E. (2012). Time-dependent movements of the hangingwall at the Kiirunavaara mine. International Journal of Mining, Reclamation and Environment. 26: 119-133.

[32]. Sui, W., Zhang, D., Chi, Z.C., Wu, Z. and Zhao, Q. (2015). Environmental implications of mitigating overburden failure and subsidences using paste-like backfill mining: a case study. International Journal of Mining, Reclamation and Environment. 29: 521-543.

[33]. Hindistan, M.A. and Yetisen, H. (2012). Assessment of subsidence at Çayırhan lignite mine using aerial photogrammetry. International Journal of Mining, Reclamation and Environment. 26: 351-365.

[34]. Deng, J., Bian, L., Li, X.B., Zhao, G.Y. and Wang, X.M. (2006). Analysis of factors and countermeasures of mining subsidence in Kaiyang Phosphorus Mine. Journal of Central South University of Technology. 13 (6): 733-737.

[35]. Salamon, M.D.G. (1984). Energy considerations in rock mechanics: fundamental results fundamental results. The South African Institute of Mining Metallurgy. 84 (8): 233-246.

[36]. Zhang, T., Ma, M., Wang, H. and Xu, H. (2011). A nonlinear rheological model of backfill material for retaining roadways and the analysis of its stability. Mining Science and Technology (China). 21: 543-546.

[37]. Salamon, M.D.G. (1990). Mechanism of caving in longwall coal mining MDG Salamon. In Rock Mechanics Contributions and Challenges: Proceedings of the 31st US Symposium on Rock Mechanics. CRC Press. pp. 161-168.

[38]. Yavu, H. (2004). An estimation method for cover pressure re-establishment distance and pressure distribution in the goaf of longwall coal mines. International Journal of Rock Mechanics & Mining Sciences. 41 (2): 193-205.

[39]. Rafiqulislam, M.D., Hayashi, D. and Kamruzzaman, A.B.M. (2009). Finite element modeling of stress distributions and problems for multi-slice longwall mining in Bangladesh, with special reference to the Barapukuria coal mine. International Journal of Coal Geology. 78: 91-109.

[40]. Khoshjavan, S., Mazlumi, M., Rezai, B. and Rezai, M. (2010). Estimation of hardgrove grindability index (HGI) based on the coal chemical properties using artificial neural networks. Oriental Journal of Chemistry. 26: 1271-1280.

[41]. Sayadi, A.R., Tavassoli, S.M.M., Monjezi, M. and Rezaei, M. (2014). Application of neural networks to predict net present value in mining projects. Arabian Journal of Geosciences. 7: 1067-1072.

[42]. Rajabi, M., Rahmannejad, R., Rezaei, M. and Ganjalipour, K. (2017). Evaluation of the maximum horizontal displacement around the power station caverns using artificial neural network. Tunnelling and Underground Space Technology. 64: 51-60.

تحلیل پایداری دراز مدت ناحیه تخریب شده در معدنکاری جبهه کار طولانی با استفاده از نظریه حداقل انرژی پتانسیل

محمد رضائی

گروه مهندسی معدن، دانشکده مهندسی، دانشگاه کردستان، ایران

ارسال ۲۰۱۷/۶/۲۹، پذیرش ۲۰۱۷/۸/۱۹

نویسنده مسئول مکاتبات: m.rezaei@uok.ac.ir

چکیده:

برآورد ارتفاع ناحیه‌های تخریب و شکست شده بالای پهنه جبهه کار طولانی و شرایط پایداری منطقه تخریب شده به منظور ارزیابی تنش‌های اطراف، نشست سطح زمین، پایداری جبهه کار، طراحی ورودی‌های اطراف و پایه‌ها بسیار حیاتی است. تخمین دراز مدت ارتفاع ناحیه تخریب- شکست به عنوان ناحیه رها شده از تنش دارای نقشی اساسی در تعیین دقیق حداکثر نشست سطح زمین و مقدار بار انتقالی به ساختارهای اطراف است. از این رو در این تحقیق مدلی جدید برای تحلیل پایداری مواد تخریب شده توسعه داده شده است. در مدل پیشنهادی، ابتدا مدل تحلیلی بر پایه روش انرژی برای تعیین ارتفاع زون رها از تنش در دراز مدت تعیین شده و سپس شرایط پایداری ناحیه تخریب شده با استفاده از اصل حداقل انرژی پتانسیل مورد بررسی قرار گرفته است. بر اساس داده‌های واقعی جمع‌آوری شده از منابع منتشر شده قبلی، زمان ناپایداری این سیستم محاسبه شده است. علاوه بر این، به منظور دست‌یابی به درک صحیحی از نقش پارامترهای مختلف، ارتباط ارتفاع ناحیه رها شده از تنش با متغیرهای زمان و ضرایب ثابت وابسته به دما مورد ارزیابی قرار گرفته است. در انتها با استفاده از تحلیل حساسیت مشخص شد که زمان مؤثرترین پارامتر و ضریب ویسکوزیته اولیه کم تأثیرترین پارامتر بر ارتفاع زون رها از تنش است. از ارتفاع ناحیه رها شده از تنش و زمان پایداری برآورد شده به ترتیب می‌توان در تعیین تنش ناشی از معدنکاری و حداکثر نشست ایجاد شده در سطح زمین استفاده کرد.

کلمات کلیدی: استخراج جبهه کار طولانی، ناحیه رها شده از تنش، سیستم مواد تخریب شده، حداقل انرژی پتانسیل، زمان پایداری.